# Creating stable Floquet–Weyl semimetals by laser-driving of 3D Dirac materials

Hannes Hübener[1], Michael A. Sentef[2], Umberto De Giovannini[1,3], Alexander F. Kemper[4] & Angel Rubio[1,2]

Tuning and stabilizing topological states, such as Weyl semimetals, Dirac semimetals or topological insulators, is emerging as one of the major topics in materials science. Periodic driving of many-body systems offers a platform to design Floquet states of matter with tunable electronic properties on ultrafast timescales. Here we show by first principles calculations how femtosecond laser pulses with circularly polarized light can be used to switch between Weyl semimetal, Dirac semimetal and topological insulator states in a prototypical three-dimensional (3D) Dirac material, $Na_3Bi$. Our findings are general and apply to any 3D Dirac semimetal. We discuss the concept of time-dependent bands and steering of Floquet–Weyl points and demonstrate how light can enhance topological protection against lattice perturbations. This work has potential practical implications for the ultrafast switching of materials properties, such as optical band gaps or anomalous magnetoresistance.

[1] Nano-Bio Spectroscopy Group and ETSF, Universidad del País Vasco, CFM CSIC-UPV/EHU, San Sebastián 20018, Spain. [2] Max Planck Institute for the Structure and Dynamics of Matter and Center for Free Electron Laser Science, Hamburg 22761, Germany. [3] Dipartimento di Fisica e Chimica, Universitá degli Studi di Palermo, Via Archirafi 36, I-90123, Palermo, Italy. [4] Department of Physics, North Carolina State University, Raleigh, North Carolina 27695-8202, USA. Correspondence and requests for materials should be addressed to H.H. (email: hannes.huebener@gmail.com) or to A.R. (email: angel.rubio@mpsd.mpg.de).

Creating and controlling phases of matter is a central goal of condensed matter physics. Recent advances in ultrafast spectroscopy[1,2] open a route towards engineering new phases with pump laser fields acting on a solid to form emergent light-matter coupled states. As an example, circularly polarized light has been shown to open a band gap and produce Floquet–Bloch states on the surface of an equilibrium topological insulator[3,4] and form a Floquet–Chern insulating state in graphene in the limit of continuous driving[5,6] and for finite pulse durations[7]. The discovery of topological states in Dirac materials has triggered a lot of interest in particular in emergent Dirac[8], Weyl[9] and Majorana fermions[10,11]. Topological states of matter are controlled by symmetries[12–14]. Traditionally, the symmetries of materials can be influenced only to a certain extent and only on slow timescales via strain, doping or static magnetic or electric fields. By contrast, Floquet engineering[15] allows to dynamically break symmetries and modify the topology of band structures[16] on ultrafast timescales.

Massless fermions in 3D Dirac and Weyl semimetals have recently attracted considerable interest. Examples include the Dirac semimetal materials $Na_3Bi$[17,18] and $Cd_3As_2$[19–25] and the Weyl semimetal states in transition-metal monophosphides[26–28], first discovered in TaAs[29–35]. Besides the fundamental importance of Weyl semimetal materials as condensed matter realizations of elementary Weyl fermions, this interest is also due to the intrinsic stability of 3D Weyl points (WPs), which are chiral and host left- or right-handed Weyl fermions, giving rise to unusual material properties, such as negative magnetoresistance[36–38], huge magnetoresistance[39] or the anomalous Hall effect[40–43]. WPs can alternatively be viewed as magnetic monopoles in momentum space with positive or negative chiral charges and host non-zero Chern numbers for some closed momentum space surfaces[13,14]. The topological protection of massless fermions in a Weyl semimetal against weak perturbations is controlled by the WP splitting in the Brillouin zone[44], as the chiral WPs can only be destroyed by chirality mixing, which requires two opposite chirality WPs to meet[26]. The massless fermions in a Dirac semimetal, by contrast, require additional crystal symmetries to be stable and are destroyed, for instance, by breaking rotational symmetry[17].

Here we propose a route towards ultrafast Floquet engineering of laser-induced topologically stable WPs starting from the 3D Dirac semimetal $Na_3Bi$ by ab initio electronic structure calculations using time-dependent density functional theory (TDDFT)[45,46]. We show that a Floquet–Weyl semimetal is dynamically created by breaking time-reversal symmetry. This symmetry breaking is achieved by applying circularly polarized classical laser fields with varying field strengths. Importantly, our strategy goes beyond the use of model tight-binding Hamiltonians and light coupling via Peierls substitution, as the TDDFT scheme automatically deals with the electronic properties and dynamical screening of the material and includes both Peierls phases for hopping terms and intra-atomic dipole (and higher multipole) transitions on equal footing[47]. In fact our theoretical framework shows effects that are not captured by simple four band models. For example, the splitting of degenerate Dirac bands into bands supporting a Floquet–Weyl point under a pump field does not occur symmetrically in all cases as would be predicted by models, and under linearly polarized pumping, the dynamical electron–electron interaction can induce a symmetry breaking field that destroys the Dirac point and opens a gap.

## Results

**Theory**. To illustrate the basic idea behind the concept of dynamically driven Floquet–Weyl semimetal, we briefly discuss the minimal model in which Floquet WPs arise from a 3D Dirac point and then move to a fully ab initio description of the real material $Na_3Bi$, where the dynamical electronic interactions of all valence electrons in the full Brillouin zone are taken into account. In a 3D Dirac semimetal, the Dirac point is a fourfold degenerate state at the Fermi level, and the low energy bands around this point obey a massless Dirac equation. Solutions to the massless Dirac equation are composed of two Weyl fermions with opposite chiralities, and the massless $4 \times 4$ Dirac Hamiltonian can be written as a combination of uncoupled left- and right-handed $2 \times 2$ Weyl Hamiltonians,

$$\hat{H}_{\mathrm{Dirac}}(\mathbf{k}) = \begin{pmatrix} \hat{H}_{\mathrm{Weyl}}(\mathbf{k}) & 0 \\ 0 & \hat{H}_{\mathrm{Weyl}}(\mathbf{k})^* \end{pmatrix}, \quad H_{\mathrm{Weyl}}(\mathbf{k}) = v_{\mathrm{F}}\mathbf{k} \cdot \boldsymbol{\sigma},$$

$$(1)$$

where $v_{\mathrm{F}}$ is the Fermi velocity, $\boldsymbol{\sigma} = (\sigma_x, \sigma_y, \sigma_z)$ are Pauli pseudospin matrices, $\mathbf{k}$ measures momentum relative to the Dirac point and $\hat{H}_{\mathrm{Weyl}}(\mathbf{k})$ is a right-handed Weyl Hamiltonian, while $\hat{H}_{\mathrm{Weyl}}(\mathbf{k})^*$ is its left-handed (time-reversed) partner, leading to eigenspinors with definite chirality. The 3D Dirac point thus consists of two degenerate WPs. In this case, the chiralities compensate each other because the WPs are at the same point in momentum space. Moreover, the WPs in a 3D Dirac semimetal are destroyed by any chirality-mixing perturbation that leads to a hybridization of the subblocks in equation (1). By contrast, in a Weyl semimetal the left- and right-handed WPs are split in momentum space and are thus not susceptible to chirality-mixing perturbations.

Starting from a 3D Dirac semimetal, see Fig. 1a, one can induce phase changes by lifting the fourfold degeneracy of the 3D Dirac point, either by introducing a mass term or by separating the degenerate WPs in momentum space. A mass term in the Dirac equation opens a gap and can stem from breaking rotational symmetry as induced by applying strain, leading to a topological insulator[17]. The separation of the WPs into a Weyl semimetal state can be achieved by breaking time-reversal symmetry via an external driving, as shown in Fig. 1b. For the sake of the simplicity of the model but without losing generality, we introduce the coupling to a time-dependent external gauge field by Peierls substitution in equation (1), which amounts to $\mathbf{k} \to \mathbf{k} - \mathbf{A}(t)$, where $\mathbf{A}$ is the time-dependent vector potential of the applied circularly polarized light, for example, $\mathbf{A}(t) = A_0(0, \cos(\Omega t), \sin(\Omega(t)))$ for polarization in the $y$–$z$ plane. This treatment only takes into account the electric field of the laser pulse and neglects its magnetic component, which is negligible here but can also be straightforwardly included in the ab initio calculation. The resulting time-dependent Hamiltonian $H(t) = H(\mathbf{k} - \mathbf{A}(t))$ describes the dynamics of the driven model system. From here on, we suppress the momentum argument $\mathbf{k}$ for brevity.

After transient effects have decayed, the system is in a stationary but non-equilibrium state of light-matter coupling that is periodic in time. Such a state can be analysed by Floquet theory, where the time dependence is described by mapping to a Hilbert space of time-independent multi-photon Hamiltonians, each projected onto a multiple of the photon frequency, effectively a Fourier–Bloch decomposition:

$$\mathcal{H}^{mn} = \frac{\Omega}{2\pi} \int_T \mathrm{d}t\, e^{i(m-n)\Omega t} H(t) + \delta_{mn} m\Omega \mathbf{1} \qquad (2)$$

where the integers $m$ and $n$ define the multi-photon Hilbert space (see Methods). This provides an interpretation of the time dependence in terms of time-independent multi-photon states with a well-defined quasi-energy band structure, the
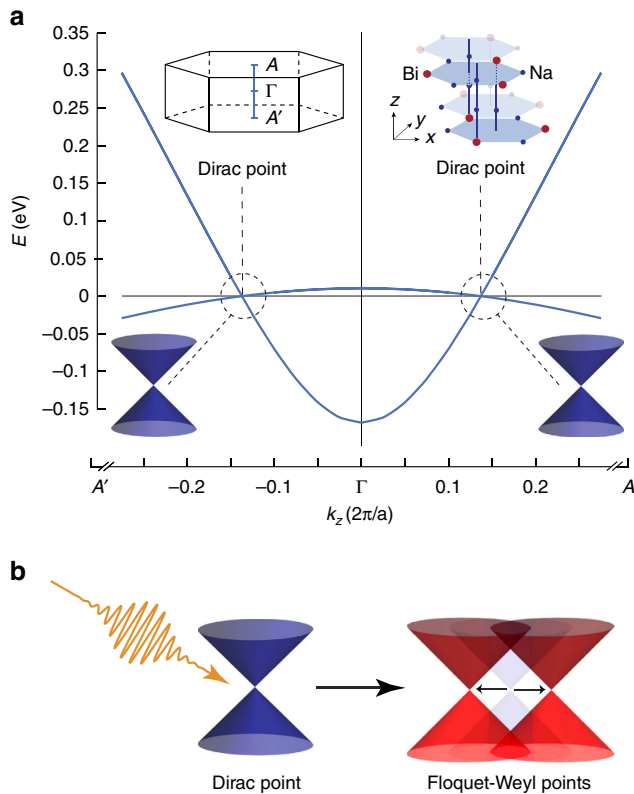
## a



## b



**Figure 1 | Laser-induced Floquet–Weyl semimetal.** (**a**) With intact time-reversal symmetry, doubly degenerate 3D Dirac cones exists at two Dirac points in Na₃Bi. Shown are the Dirac bands along a section of the $A' - \Gamma - A$ path through the Brillouin zone, see left inset. The right inset shows the crystal structure of Na₃Bi. (**b**) Breaking time-reversal symmetry with circularly polarized light splits each Dirac cone into a pair of Floquet–Weyl cones.

3D Dirac semimetals and has the same dependence on amplitude and frequency but with a different prefactor. However, owing to asymmetry of the bands in the actual material Na₃Bi, it can also lead to a non-symmetric shift of the two WPs in energy away from the Fermi level, one upwards and the other one downwards, forming a topological Weyl metal. Thus, by controlling amplitude, polarization and envelope of the driving field, one can engineer different nontrivial Floquet topological phases. In particular, the same mechanism can be used to induce the Floquet–Weyl semimetal phase in systems that initially have a finite gap. Applying strain to a 3D Dirac semimetal opens a gap that can subsequently be closed by applying the driving field and with sufficient field strength the Weyl semimetal can be recovered, implying the possibility of Floquet engineering a non-equilibrium metal-insulator transition.

For a realistic description of the 3D-Dirac semimetal Na₃Bi (see Fig. 1) and its insulating strained version under the influence of a periodic driving field, we use the first principles formalism of TDDFT[45–47,49]. In this approach, the electronic density is propagated in real time according to the time-dependent Kohn-Sham Hamiltonian, which accounts for electron–ion and electron–electron interactions through the time-dependent Hartree and the Kohn-Sham exchange and correlation potentials. The external gauge field is naturally included in the theory up to all orders as a time-dependent phase, as are the electronic multipoles to all orders. The time-dependent electronic structure from TDDFT is then further processed using the Floquet expansion (see Methods). This Floquet TDDFT method represents a powerful and flexible tool to analyse and interpret time-dependent simulations, retaining both the rigorous *ab initio* description of the electronic ground and time-dependent excited states while allowing for the readily accessible quasi-static picture of Floquet theory. The emergent Floquet bands can be viewed as snapshots of the electronic structure, time-averaged over the fast oscillation period of the external driving field but time-resolved on the slower timescale of the pump pulse duration. This interpretation naturally reflects the measurement process in pump-probe photoemission spectroscopy[7,50].

Both the carrier acceleration via Peierls substitution and the optical dipole transitions are automatically included in the TDDFT time propagation. For example, the observed asymmetric band splitting in the Weyl metal case would not follow from a simple tight-binding model but would require including dipole transitions that are *a priori* unknown for such a model and would therefore have to be retrofitted. Moreover, by comparing the full TDDFT results including the exchange-correlation potential with a noninteracting time propagation, we find that the induced Hartree and exchange-correlation potentials do not have a crucial role for the effects described in this paper. Hence, the results are indeed generic. However, we stress that, for different setups and effects beyond the ones discussed here, electron–electron or electron–phonon interactions may indeed become important and will be accounted for by our theoretical approach. The Floquet TDDFT framework introduced here will equally well apply to these situations and many more.

In the picture of photon-dressed states, Floquet sidebands are created as replicas of the original bands, spaced by the photon energy and periodically repeated in quasi-energy, in an enhanced Hilbert space including multiphoton processes. In practice, these replicas will be observed if the sidebands are occupied[3,7], but they do not influence the physics discussed in this paper, in contrast to a different recent proposal for emergent Floquet–Weyl points at sideband crossings[51]. Importantly, the main effect exploited in our work is due to off-resonant photon absorption, which is why the photon frequency is a freely tunable parameter that allows one to move the Floquet sidebands, for instance,

Floquet bands. In the high-frequency limit, one can decouple the zero-photon dressed states from the other states, amounting to a simple time average, and add multi-photon states perturbatively[5,48],

$$\hat{H}_{\text{eff}} = \mathcal{H}^{00} + \frac{1}{\Omega}\left[\mathcal{H}^{0-1}, \mathcal{H}^{01}\right]. \tag{3}$$

where $\mathcal{H}^{00}$ is the zero order (cycle-averaged) Hamiltonian and $\mathcal{H}^{0\pm1}$ are the single photon dressed Hamiltonians, c.f equation (2). This Floquet downfolding has the advantage that one recovers the original Hilbert space of the electronic system and the resulting effective Hamiltonian $\hat{H}_{\text{eff}}$ of this simple model retains an analytical form. Thus, for the the Dirac Hamiltonian, equation (1), and $y–z$ circularly polarized light, the downfolded effective Floquet–Hamiltonian reads

$$\hat{H}_{\text{eff}} = \begin{pmatrix} \hat{H}_{\text{Weyl}}(\mathbf{k}) + \frac{(v_{\text{F}}A_0)^2}{\Omega}\sigma_x & 0 \\ 0 & \hat{H}_{\text{Weyl}}(\mathbf{k})^* - \frac{(v_{\text{F}}A_0)^2}{\Omega}\sigma_x \end{pmatrix} \tag{4}$$

The effective gauge field acts on the the *x*-component of the wave vector and results in a shift in the position of each of the originally degenerate WPs by $\pm(v_{\text{F}}A_0)^2/\Omega$ along the $k_x$ direction in momentum space creating a Floquet–Weyl semimetal. This mechanism of light-induced effective gauge fields that alters the topology of the material is the central effect discussed in this paper. By solving the full *ab initio* mutli-photon Floquet–Hamiltonian without resorting to a high-frequency expansion or model parameters, we show that this effect occurs in real

if sidebands from other bands further away from the Fermi level happened to interfere with the Floquet–Weyl points.

**Floquet–Weyl points induced by circularly polarized light.** Applying time-reversal symmetry breaking fields to a 3D Dirac material lifts the degeneracy of the Dirac point into WPs leading to two distinct Floquet–Weyl cones emerging from each Dirac point in the Brillouin zone. In Fig. 2, we illustrate this effect using circularly polarized light with two different polarization planes. Although the $k_x$ and $k_y$ directions in the Brillouin zone of $Na_3Bi$ are equivalent, and both showing symmetrical Dirac cones in the equilibrium phase, the dispersion of the Dirac cone along the $k_z$ direction is asymmetric[17], see Fig. 1a. This leads to qualitatively different behaviour of the driven system along the $k_z$ direction as opposed to the symmetric effect in the $x$–$y$ plane. Circularly polarized light in the $y$–$z$-plane splits the the Floquet WPs along the $k_x$ direction forming a Floquet–Weyl semimetal, as shown in Fig. 2c. Conversely, with light polarized in the $x$–$y$ plane the Floquet WPs split along the $k_z$ direction, cf. Fig. 2f.

Owing to the asymmetry of the equilibrium Dirac cone along $k_z$, the Floquet WPs are not only split horizontally but also shift vertically away from the Fermi energy. Crucially, one Floquet WP moves to positive energies while the other one is shifted below the Fermi energy. The resulting complex intersection of the two Floquet–Weyl cones is shown in Fig. 2e. The shift in energy of the Floquet WPs leads to the opening of two Fermi surfaces around these Floquet WPs with opposing Chern numbers owing to the opposite chiralities of the enclosed Floquet WPs[17].

**Steering Floquet–Weyl points.** In a pump-probe experiment, there are two different timescales at play, the time of the period of oscillation and the time of the modulation of the amplitude owing to the shape of the pump pulse. The pump duration is typically orders of magnitude longer than the oscillation of the field and hence the pulse shape has no effect on the formation of Floquet–Weyl points at any given time during the pumping. In our calculations, we observe that the Floquet limit is reached after two cycles of the driving field, and thus this assumption
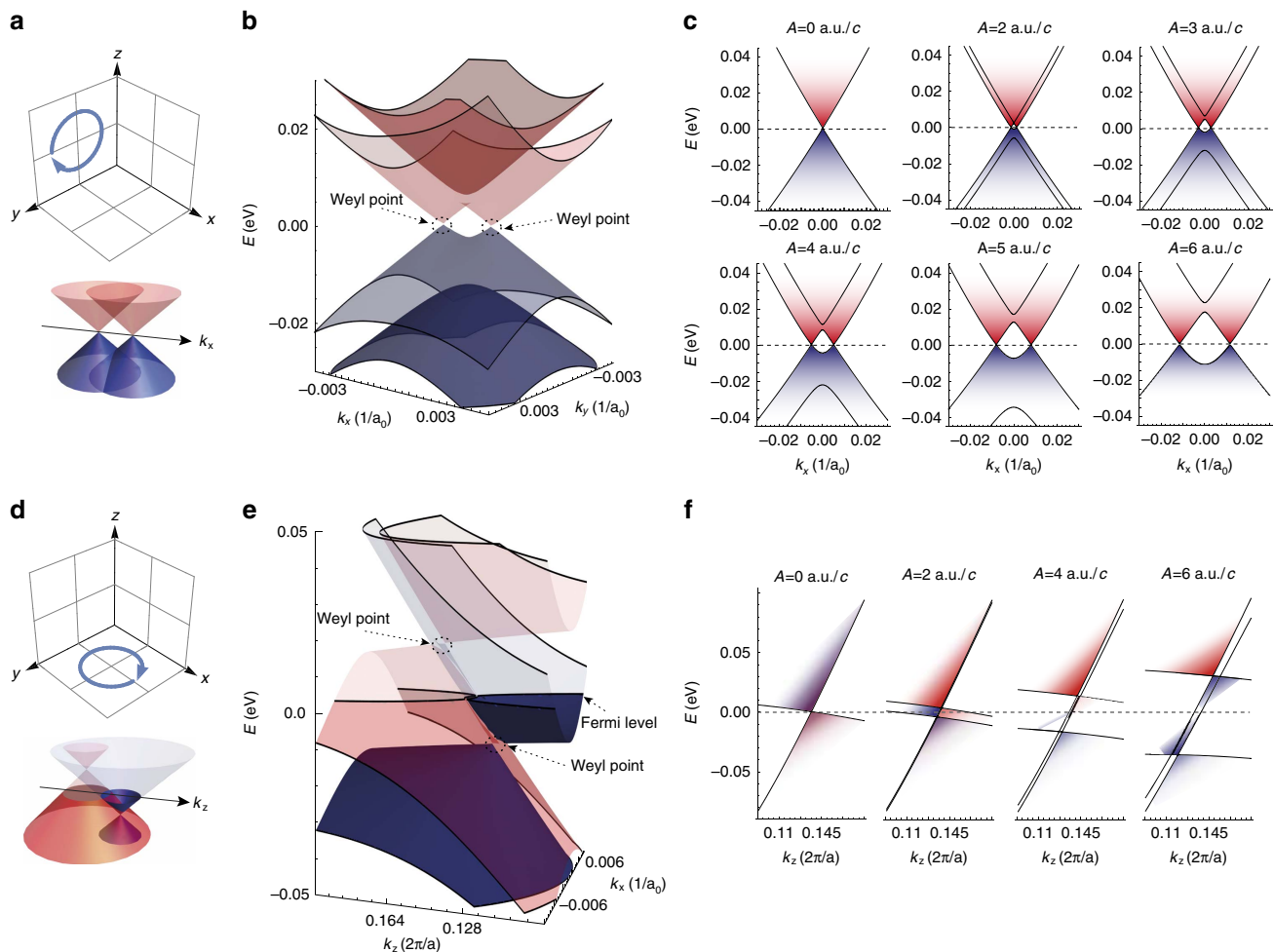


**Figure 2 | Polarization control of Floquet–Weyl point splitting.** (**a**) Circularly polarized light in the $y$–$z$-plane splits Floquet–Weyl points along the $k_x$ direction at the Fermi level, resulting in a Floquet–Weyl semimetal. (**b**) The Floquet–Weyl points form 3D cones in the Brillouin zone. An example in the $k_x$–$k_y$-plane is shown for amplitude $A = 3$ a.u./$c$. (**c**) The splitting of the Floquet–Weyl points increases with the intensity (amplitude) of the driving field. Here we show the effect of different amplitudes $A$ of a field with photon energy $\hbar\Omega = 1.5$ $eV$ in momentum cuts around the Dirac point along $k_x$. The units of the amplitude of the vector potential can be translated to electric field strength in units of V/Å, see Methods. (**d**) With a similar driving field, but polarized in the $x$–$y$-plane, the Floquet–Weyl points split along the $k_z$ direction, but in this case move away from the Fermi level, as shown in (**f**) for a series of amplitudes. (**e**) Shows how this leads with an amplitude of $A = 4$ a.u./$c$ to an opening of topological Fermi surfaces (rings in the $k_x$–$k_z$ plane) around the Floquet–Weyl points and a complex intersection of the Floquet–Weyl cones. In all panels, the Fermi level is at zero energy.
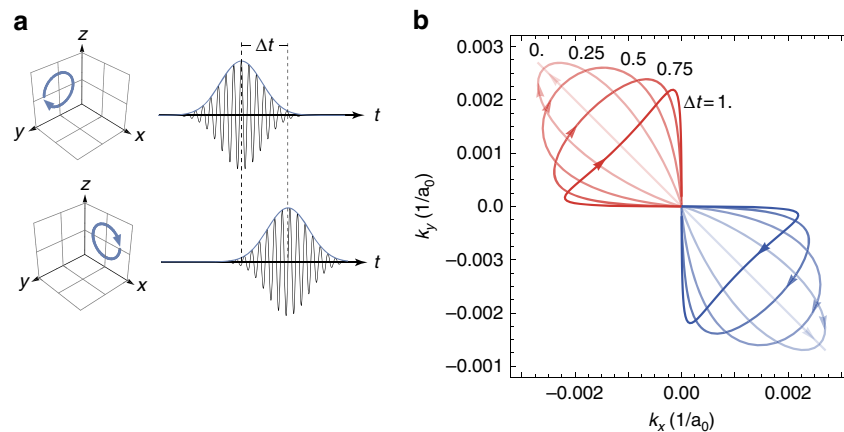
**Figure 3 | Dynamical Floquet–Weyl points. (a)** Floquet TDDFT predicts that the position of the Floquet–Weyl points can be controlled in real time on the timescale of pulse envelopes, yielding a time-dependent band structure that is accessible through time- and angle-resolved photoemission spectroscopy. Two time-delayed ($\Delta t$) pump laser pulses, circularly polarized in $y$–$z$ and $x$–$z$ directions, respectively, drive the Floquet–Weyl points in the $k_x$–$k_y$ plane of the BZ. **(b)** The varying field strength during the laser pulses leads to dancing Floquet–Weyl points with trajectories controlled by $\Delta t$ given in units of the FWHM of pulse envelopes.

holds even for relatively short pulses of 100 fs. However, the changing of the envelope amplitude over time will change the position of the WPs according to Fig. 2. This means that on the timescale of the pump envelope there is a movement of the WPs through the Brillouin zone. Furthermore, from the previous discussion it has become clear that combining different pump polarization offers the possibility to control the position of the Floquet WPs within the Brillouin zone. Thus, by modulating the amplitudes of two pump fields, that is, by controlling the delay between two pump pulses, one can time-dependently steer the Floquet WPs. Figure 3 shows how a simple time delay between two Gaussian pump pulses in the $x$–$z$ and $y$–$z$ planes controls complex trajectories of the two Floquet WPs through the Brillouin zone. With more sophisticated combinations of different pump envelopes, one can design complex dynamics of Floquet WPs on the timescale of the pulse duration. Thus Floquet TDDFT also provides a way of analysing time-dependent band structures that are different from the instantaneous eigenvalues of the TDDFT Hamiltonian and that can be measured using time-resolved photoemission spectroscopy, which has an intrinsic time-averaging procedure given by the probe pulse shape[7]. We also remark here that, in principle, further replicas of the dancing Floquet WPs may be observed as an effect of Floquet sideband formation.

**Strain**. In all Dirac metals, the doubly degenerate 3D Dirac point of the equilibrium phase of the material leaves the topology unstable under small lattice deformations. In Na$_3$Bi, already a small strain breaks the rotational $\mathcal{C}_3$ symmetry and leads to an opening of a gap owing to chirality mixing and the formation of a topological insulator phase[17], Fig. 4a. The Floquet WPs, however, are protected by conservation of chirality and afford the system topological protection. In fact, for an initially gapped system, the application of the driving field can lead to a restoration of the topology and the Floquet–Weyl semimetal phase. In Fig. 4b, the progression from the strained gapped topological insulator phase to the Floquet–Weyl semimetal phase is shown as the amplitude of the driving field increases. The transition from one phase to the other occurs at a critical amplitude that characterizes a phase boundary in a Floquet phase diagram, see Fig. 4c. We note that a related idea was used to

drive a topological insulator into a Weyl semimetal phase in ref. 52.

Besides being a striking illustration of the power of topological protection, this light-induced phase transition might also be of technological relevance, because it facilitates light-controlled, ultrafast switching between an insulating and metallic phase. In particular, when the driving field is circularly polarized in the $x$–$y$ plane the topological insulator phase can be switched to a phase with non-trivial topological Fermi surfaces, possibly allowing for a technological exploitation of the exotic transport phenomena encountered in this phase[38,39].

**Discussion**

Our work demonstrates how topological properties in solids can be Floquet engineered. Floquet TDDFT predicts distinct Weyl semimetal, Weyl metal and topological insulator Floquet band structures that can be measured with time-resolved photoemission spectroscopy. The splitting of Floquet–Weyl points controlled by laser driving illustrates how the concept of separation of chiral particles in momentum space inspires the Floquet engineering of topologically stable states. Regarding anomalous transport properties, we envision that THz magneto-transport might be able to detect effects of Floquet–Weyl fermions near the Fermi level, for instance, the anomalous negative magnetoresistance corresponding to the chiral Adler–Bell–Jackiw anomaly[36–38], the recently demonstrated chiral magnetic effect[53], a proposed chiral pumping effect with an axial current[54] or huge magnetoresistance for the Floquet–Weyl metal with hole and electron Fermi surfaces[39] arising for $x$–$y$ polarization. Our predictions can be directly checked in pump-probe angle-resolved photoemission experiments, which can measure the transient Floquet band structures[3,4]. These experiments could additionally even provide evidence about topological features implied by topological insulator, Dirac semimetal and Weyl semimetal materials, for example, Fermi arc surface states of Weyl semimetal or surface states in topological insulators. Furthermore, a recent work[55] proposes measurement of the Wigner distribution as a means to identify non-trivial Floquet phases.

In terms of method development, we have introduced the framework of Floquet TDDFT as a tool for the first principles prediction of Floquet engineered bands and topologies.
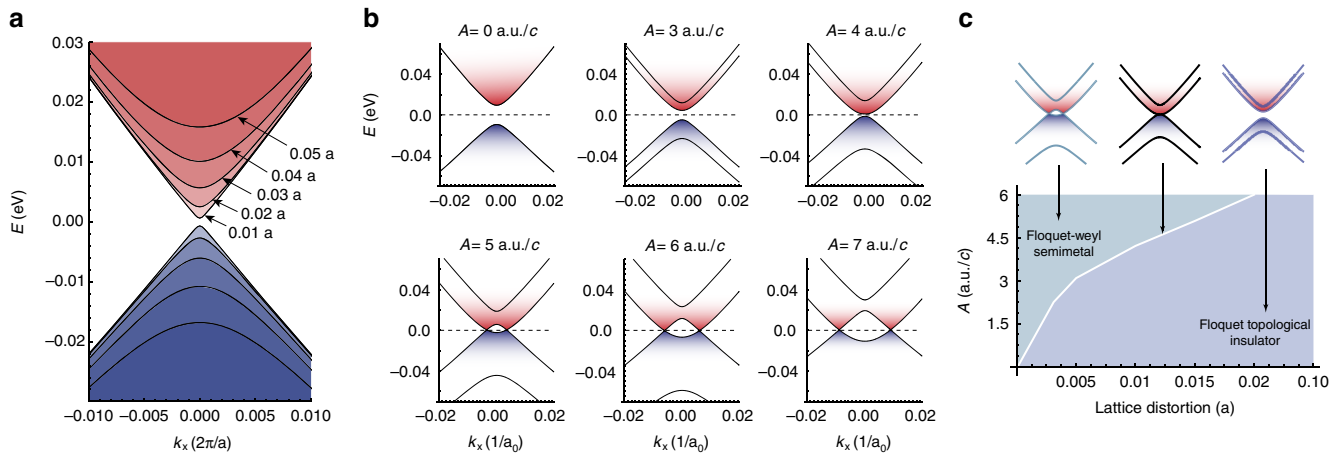
**Figure 4 | Floquet topological phase transition and enhanced topological protection. (a)** In strained samples, the breaking of crystal symmetries opens a gap at the 3D Dirac point, leading to a topological insulator phase. In Na$_3$Bi, strain along x breaks the $C_3$ symmetry. Shown is a series of band structures for different lattice distortions measured as a fraction of the lattice parameter. **(b)** The strain-induced band gaps can be closed by the application of circularly polarized light. For 1% lattice distortion, increasing the amplitude of a y–z circularly polarized driving field with $\hbar\Omega = 1.5$ eV first reduces the gap, then closes it at a critical amplitude $A_c$ and restores the Floquet–Weyl semimetal observed in the unstrained case (see Fig. 2c). The units of the amplitude of the vector potential can be translated to electric field strength in units of V/Å. **(c)** This light-induced Floquet topological phase transition from topological cycle insulator to Weyl semimetal defines a non-equilibrium phase diagram as a function of amplitude and lattice distortion for a given driving field frequency.

Furthermore, it provides a setting to discuss time-dependent band structures on timescales accessible in pump-probe experiments. Finally, electron correlation effects beyond independent particles in driven systems are thus within reach, paving the way for the study of nonlinear laser field and collective excitation effects, such as the coupling to phonons, or exciton and plasmon formation in realistic Floquet-driven complex materials.

## Methods

**Units of field amplitudes.** The amplitudes of the vector potentials discussed in the text can be converted to electric field strength as $E = -\partial A/\partial t \sim -A\Omega$ assuming that the envelope is constant. This leads to a conversion of 1 [a.u./c] = 0.013789 V/ÅΩ eV. For the frequency of $\hbar\Omega = 1.5$ eV used here, this corresponds to a conversion of all amplitudes A given in the text as 1 [a.u./c] = 0.0206849 V/Å = 2.068498 MV cm$^{-1}$.

**Floquet TDDFT.** According to the Floquet theorem, the solutions of the time-dependent Schrödinger equation $i\partial_t|\psi(t)\rangle = \hat{H}(t)|\psi(t)\rangle$ with a Hamiltonian that is periodic in time, that is, $\hat{H}(t+T) = \hat{H}(t)$, can be obtained by computing the eigenstates of a static Hamiltonian in the Hilbert space of multi-photon dressed states. This static Hamiltonian follows from performing a Floquet–Bloch expansion of the time-dependent solutions of the Schrödinger equation $|\psi(t)\rangle = \sum \exp(-i(\epsilon + m\Omega)t)|u_m\rangle$, where $\Omega = 2\pi/T$, $\epsilon$ is the Floquet quasi-energy, and $|u_m\rangle^m$ is the corresponding mth Floquet eigenfunction, which does not depend on time. The time-dependent Schrödinger equation then reduces to the static equation

$$\sum_n \mathcal{H}^{mn}|u_n\rangle = \epsilon|u_m\rangle \quad (5)$$

for each $\epsilon$, where the $\mathcal{H}^{mn}$ is a static Hamiltonian

$$\mathcal{H}^{mn} = \frac{1}{T}\int_T dt\, e^{i(m-n)\Omega t}H(t) + \delta_{mn}m\Omega\mathbf{1} \quad (6)$$

defined in the infinite Hilbert space of multi-photon (that is, multiples of $\Omega$) components. Thus Floquet theory offers a way of analysing periodically driven systems. In principle, the full description of the system requires the diagonalization of the full Floquet–Hamiltonian while in practice one truncates the photon number depending on the problem at hand. In this work, we found that the contributions of two-photon terms and beyond had a negligible effect on the bands considered here.

The motivation to perform Floquet analysis is to project the time dependence of the driven system to a static picture. Although this is usually used to obtain an analytical expression that exposes the physical mechanism, we use it here literally as a tool to analyse time-dependent data. TDDFT gives the real-time evolution of the electronic density by propagating the Kohn-Sham states under any kind of

static or time-dependent perturbation. The time evolution operator is built from the Kohn-Sham Hamiltonian $H_{KS}$ with explicitly time-dependent external fields $V_{ext}$:

$$H_{KS}(t) = T + V_0 + V_H[n(t)] + V_{xc}[n(t)] + V_{ext}(t) \quad (7)$$

where T and $V_0$ are the kinetic energy and static potential, while the Hartree potential $V_H$ and the exchange and correlation potential $V_{xc}$ dynamically depend on the density $n(t)$ during the time evolution. For extended systems, we use the velocity gauge concept introduced in ref. 47 to treat, within the dipole approximation, the response of extended periodic systems to an arbitrary time-dependent perturbation. Within the velocity gauge, the external potential arises in the Hamiltonian from the substitution $\mathbf{p} \rightarrow \mathbf{p} - \mathbf{A}(t)/c$ leading to the terms $1/2(\mathbf{p} - \mathbf{A}(t)/c)^2 = T + 1/2(A(t)/c)^2 - \mathbf{p}\cdot\mathbf{A}(t)/c = T + V_{ext}(t)$ (in atomic units).

Besides the fact that the physical properties of the system over time can then be derived from the time-dependent density, it is obvious that this approach also generates a Hamiltonian at each time step. If the system is driven by a periodic external field or finds itself in an otherwise periodically oscillating state, such as phonon modes, this Hamiltonian fulfills the Floquet condition of periodicity and can be used directly in equation (2). Hence, Floquet analysis provides an approach of processing real-time propagation results from TDDFT to obtain spectral information that is richer than the instantaneous Kohn-Sham eigenvalues.

In practice, the Floquet TDDFT requires storing the time-dependent Hamiltonian, not just its instantaneous eigenvalues, during one cycle of periodicity so it can be used in the time integral of equation (2). This would require an unfeasible amount of storage for most systems in a real-space or wavevector basis. Instead, it is sufficient to save either the time-dependent density or the implicitly time-dependent potentials $V_{xc}$ and $V_H$. It is also worth noting that, as the evolution of the system is smooth, the time integrals in equation (2) can be evaluated with a coarse time sampling of the Hamiltonian. Furthermore, the Floquet condition of periodicity does not have to be fulfilled a priori but one can perform the Floquet analysis over any time interval corresponding to the cycle of periodicity and determine the Floquet limit as a convergence of the Floquet bands with propagation time.

We note that, in the Floquet TDDFT results, we always observe a small shift of the energies of maximum 20 meV for large amplitudes that we assign to numerical inaccuracies. This shift does not change the character of the Weyl semimetal phase, because it just corresponds to the case of a doped Weyl semimetal, and therefore we have compensated it in the all the figures.

The fully ab initio nature of Floquet TDDFT means that it requires no fitting reference. Instead, it might indeed be used as a reference itself for simplified qualitative tight-binding models that reduce the observed effect to its essential ingredients. For example, one might think of using such an approach to refine the illustrative model we use in equation (1). Although this can be useful in some case one, however, loses the quantitative accuracy that TDDFT provides and in this case leads to quantitatively wrong dynamics of the WPs.

**Computational details.** We carry out DFT and TDDFT calculations as implemented in the OCTOPUS code[49] using the (adiabatic) local density approximation and Hartwigsen-Goedecker-Hutter (HGH) pseudopotenitals,[56] including spin-orbit coupling. The structure is taken from ref. 17 where the lattice parameter is given as $a = 10.2952271$ Bohr. The groundstates are computed with a $10 \times 5 \times 5$ Monkhorst–Pack Brillouin zone sampling and a real-space mesh of 0.3 Bohr spacing. The TDDFT calculations are performed with a time step of $0.05\,\hbar\,Ha^{-1}$ and with a uniform external vector potential oscillating with a frequency of $\hbar\Omega = 1.5\,eV$ and with different amplitudes specified in the text. We find that, for our calculations of Na$_3$Bi, the Floquet band structures do not depend on the local density approximation functional and also the effect of the induced Hartree potential is negligible for circular polarized driving fields. The code to perform non-interacting Floquet TDDFT is part of the OCTOPUS code.

**Code availability.** The OCTOPUS code is available from http://www.octopus-code.org.

**Data availability.** Data generated for this work have been deposited in the NoMaD repository (DOI: http://dx.doi.org/10.17172/NOMAD/2016.11.07-1) (ref. 57).

# References

1. Orenstein, J. Ultrafast spectroscopy of quantum materials. *Phys. Today* **65**, 44–50 (2012).
2. Zhang, J. & Averitt, R. Dynamics and control in complex transition metal oxides. *Annu. Rev. Mater. Res.* **44**, 19–43 (2014).
3. Wang, Y. H., Steinberg, H., Jarillo-Herrero, P. & Gedik, N. Observation of Floquet-Bloch states on the surface of a topological insulator. *Science* **342**, 453–457 (2013).
4. Mahmood, F. *et al.* Selective scattering between Floquet-Bloch and Volkov states in a topological insulator. *Nature Physics.* **12**, 306–310 (2016).
5. Oka, T. & Aoki, H. Photovoltaic Hall effect in graphene. *Phys. Rev. B* **79**, 081406 (2009).
6. Kitagawa, T., Oka, T., Brataas, A., Fu, L. & Demler, E. Transport properties of nonequilibrium systems under the application of light: photoinduced quantum Hall insulators without Landau levels. *Phys. Rev. B* **84**, 235108 (2011).
7. Sentef, M. A. *et al.* Theory of Floquet band formation and local pseudospin textures in pump-probe photoemission of graphene. *Nat. Commun.* **6**, 7047 (2015).
8. Novoselov, K. S. *et al.* Two-dimensional gas of massless Dirac fermions in graphene. *Nature* **438**, 197–200 (2005).
9. Nielsen, H. B. & Ninomiya, M. The Adler-Bell-Jackiw anomaly and Weyl fermions in a crystal. *Phys. Lett. B* **130**, 389–396 (1983).
10. Kitaev, A. Y. Unpaired Majorana fermions in quantum wires. *Phys. Usp.* **44**, 131 (2001).
11. Fu, L. & Kane, C. L. Superconducting proximity effect and majorana fermions at the surface of a topological insulator. *Phys. Rev. Lett.* **100**, 096407 (2008).
12. Kitaev, A. in *AIP Conference Proceedings* **1134**, 22–30 (American Institute of Physics, 2009).
13. Hasan, M. Z. & Kane, C. L. Colloquium: topological insulators. *Rev. Mod. Phys.* **82**, 3045–3067 (2010).
14. Qi, X.-L. & Zhang, S.-C. Topological insulators and superconductors. *Rev. Mod. Phys.* **83**, 1057–1110 (2011).
15. Hänggi, P. in *Quantum Transport and Dissipation* (Wiley-VCH, 1998).
16. Lindner, N. H., Refael, G. & Galitski, V. Floquet topological insulator in semiconductor quantum wells. *Nat. Phys.* **7**, 490–495 (2011).
17. Wang, Z. *et al.* Dirac semimetal and topological phase transitions in A$_3$Bi (A = Na, K, Rb). *Phys. Rev. B* **85**, 195320 (2012).
18. Liu, Z. K. *et al.* Discovery of a three-dimensional topological dirac semimetal, Na$_3$Bi. *Science* **343**, 864–867 (2014).
19. Wang, Z., Weng, H., Wu, Q., Dai, X. & Fang, Z. Three-dimensional Dirac semimetal and quantum transport in Cd$_3$As$_2$. *Phys. Rev. B* **88**, 125427 (2013).
20. Ali, M. N. *et al.* The crystal and electronic structures of Cd$_3$As$_2$, the three-dimensional electronic analogue of graphene. *Inorg. Chem.* **53**, 4062–4067 (2014).
21. Neupane, M. *et al.* Observation of a three-dimensional topological Dirac semimetal phase in high-mobility Cd$_3$As$_2$. *Nat. Commun.* **5**, 3786 (2014).
22. Liu, Z. K. *et al.* A stable three-dimensional topological Dirac semimetal Cd$_3$As$_2$. *Nat. Mater.* **13**, 677–681 (2014).
23. Liang, T. *et al.* Ultrahigh mobility and giant magnetoresistance in the Dirac semimetal Cd$_3$As$_2$. *Nat. Mater.* **14**, 280–284 (2015).
24. Borisenko, S. *et al.* Experimental realization of a three-dimensional dirac semimetal. *Phys. Rev. Lett.* **113**, 027603 (2014).
25. Jeon, S. *et al.* Landau quantization and quasiparticle interference in the three-dimensional Dirac semimetal Cd$_3$As$_2$. *Nat. Mater.* **13**, 851–856 (2014).
26. Weng, H., Fang, C., Fang, Z., Bernevig, B. A. & Dai, X. Weyl semimetal phase in noncentrosymmetric transition-metal monophosphides. *Phys. Rev. X* **5**, 011029 (2015).
27. Huang, S.-M. *et al.* A Weyl Fermion semimetal with surface Fermi arcs in the transition metal monopnictide TaAs class. *Nat. Commun.* **6**, 7373 (2015).
28. Liu, Z. K. *et al.* Evolution of the Fermi surface of Weyl semimetals in the transition metal pnictide family. *Nat. Mater.* **15**, 27–31 (2016).
29. Xu, S.-Y. *et al.* Discovery of a Weyl fermion semimetal and topological Fermi arcs. *Science* **349**, 613–617 (2015).
30. Lv, B. *et al.* Experimental discovery of Weyl semimetal TaAs. *Phys, Rev. X* **5**, 031013 (2015).
31. Lv, B. Q. *et al.* Observation of Weyl nodes in TaAs. *Nat. Phys.* **11**, 724–727 (2015).
32. Xu, S.-Y. *et al.* Discovery of a Weyl fermion state with Fermi arcs in niobium arsenide. *Nat. Phys.* **11**, 748–754 (2015).
33. Yang, L. X. *et al.* Weyl semimetal phase in the non-centrosymmetric compound TaAs. *Nat. Phys.* **11**, 728–732 (2015).
34. Xu, N. *et al.* Observation of Weyl nodes and Fermi arcs in tantalum phosphide. *Nat. Commun.* **7**, 11006 (2016).
35. Xu, S.-Y. *et al.* Experimental discovery of a topological Weyl semimetal state in TaP. *Sci. Adv.* **1**, e1501092 (2015).
36. Zyuzin, A. A. & Burkov, A. A. Topological response in Weyl semimetals and the chiral anomaly. *Phys. Rev. B* **86**, 115133 (2012).
37. Parameswaran, S., Grover, T., Abanin, D., Pesin, D. & Vishwanath, A. Probing the chiral anomaly with nonlocal transport in three-dimensional topological semimetals. *Phys. Rev. X* **4**, 031035 (2014).
38. Huang, X. *et al.* Observation of the chiral-anomaly-induced negative magnetoresistance in 3D Weyl semimetal TaAs. *Phys. Rev. X* **5**, 031023 (2015).
39. Shekhar, C. *et al.* Extremely large magnetoresistance and ultrahigh mobility in the topological Weyl semimetal candidate NbP. *Nat. Phys.* **11**, 645–649 (2015).
40. Yang, K.-Y., Lu, Y.-M. & Ran, Y. Quantum Hall effects in a Weyl semimetal: possible application in pyrochlore iridates. *Phys. Rev. B* **84**, 075129 (2011).
41. Burkov, A. A. & Balents, L. Weyl semimetal in a topological insulator multilayer. *Phys. Rev. Lett.* **107**, 127205 (2011).
42. Hosur, P. & Qi, X. Recent developments in transport phenomena in Weyl semimetals. *C. R. Phys.* **14**, 857–870 (2013).
43. Chan, C.-K., Lee, P. A., Burch, K. S., Han, J. H. & Ran, Y. When chiral photons meet chiral fermions: photoinduced anomalous Hall effects in Weyl semimetals. *Phys. Rev. Lett.* **116**, 026805 (2016).
44. Nielsen, H. B. & Ninomiya, M. Absence of neutrinos on a lattice. *Nucl. Phys. B* **185**, 20–40 (1981).
45. Runge, E. & Gross, E. K. U. Density-functional theory for time-dependent systems. *Phys. Rev. Lett.* **52**, 997–1000 (1984).
46. Marques, M., Maitra, N., Nogueira, F., Gross, E. & Rubio, A. (eds) *Fundamentals of Time-Dependent Density Functional Theory-Lecture Notes in Physics,* Vol. 837 (Springer, 2012).
47. Bertsch, G. F., Iwata, J.-I., Rubio, A. & Yabana, K. Real-space, real-time method for the dielectric function. *Phys. Rev. B* **62**, 7998–8002 (2000).
48. Bukov, M., D'Alessio, L. & Polkovnikov, A. Universal high-frequency behavior of periodically driven systems: from dynamical stabilization to Floquet engineering. *Adv. Phys.* **64**, 139–226 (2015).
49. Andrade, X. *et al.* Real-space grids and the Octopus code as tools for the development of new simulation approaches for electronic systems. *Phys. Chem. Chem. Phys.* **17**, 31371–31396 (2015).
50. Freericks, J. K., Krishnamurthy, H. R. & Pruschke, T. Theoretical description of time-resolved photoemission spectroscopy: application to pump-probe experiments. *Phys. Rev. Lett.* **102**, 136401 (2009).
51. Zou, J.-Y. & Liu, B.-G. Floquet Weyl fermions in a circularly-polarised-light-irradiated three-dimensional stacked graphene systems. *Phys. Rev. Lett. B* **93**, 205435 (2016).
52. Wang, R., Wang, B., Shen, R., Sheng, L. & Xing, D. Y. Floquet Weyl semimetal induced by off-resonant light. *EPL (Europhys. Lett.)* **105**, 17004 (2014).
53. Li, Q. *et al.* Chiral magnetic effect in ZrTe5. *Nat. Phys* **12**, 550–554 (2016).
54. Ebihara, S., Fukushima, K. & Oka, T. Chiral pumping effect induced by rotating electric fields *Phys. Rev. B.* **93**, 155107 (2016).
55. Kolodrubetz, M., Fregoso, B. M. & Moore, J. E. Non adiabatic bulk-surface oscillations in driven topological insulators. *Phys. Rev B* **94**, 195124 (2016).
56. Hartwigsen, C., Goedecker, S. & Hutter, J. Relativistic separable dual-space Gaussian pseudopotentials from H to Rn. *Phys. Rev. B* **58**, 3641–3662 (1998).
57. Hübener, H., De Giovannini, U. & Rubio, A. Floquet-bandstructures of circular driven Na$_3$Bi. Novel Materials Discovery (NoMaD) Repository Available at http://dx.doi.org/10.17172/NOMAD/2016.11.07-1 (2016).

# Acknowledgements

## Author contributions

H.H. and M.A.S. designed the model and the computational framework and analysed the data. H.H. and U.D.G. carried out the implementation. H.H. performed the calculations. H.H. and M.A.S. wrote the manuscript with input from all authors. A.F.K. and A.R. conceived the study and were in charge of overall direction and planning.

## Additional information

**Competing financial interests:** The authors declare no competing financial interests.

**Reprints and permission** information is available online at http://npg.nature.com/reprintsandpermissions/

**How to cite this article:** Hübener, H. *et al.* Creating stable Floquet–Weyl semimetals by laser-driving of 3D Dirac materials. *Nat. Commun.* **8,** 13940 doi: 10.1038/ncomms13940 (2017).

**Publisher's note**: Springer Nature remains neutral with regard to jurisdictional claims in published maps and institutional affiliations.